

Terahertz radiation enhanced emission of fluorescence from elongated plasmas and microplasmas in the counter-propagating geometry

Fabrizio Buccheri, Kang Liu, and Xi-Cheng Zhang

Citation: *Appl. Phys. Lett.* **111**, 091103 (2017); doi: 10.1063/1.4990143

View online: <https://doi.org/10.1063/1.4990143>

View Table of Contents: <http://aip.scitation.org/toc/apl/111/9>

Published by the [American Institute of Physics](#)

Articles you may be interested in

[Observation of broadband terahertz wave generation from liquid water](#)

Applied Physics Letters **111**, 071103 (2017); 10.1063/1.4990824

[Transferring linear motion of an optical wedge to rotational frequency shift in an orbital angular momentum interferometer](#)

Applied Physics Letters **111**, 091102 (2017); 10.1063/1.4995366

[Broadband non-polarizing terahertz beam splitters with variable split ratio](#)

Applied Physics Letters **111**, 071101 (2017); 10.1063/1.4986538

[Mid-infrared epsilon-near-zero modes in ultra-thin phononic films](#)

Applied Physics Letters **111**, 091105 (2017); 10.1063/1.4996213

[Electrical dynamic modulation of THz radiation based on superconducting metamaterials](#)

Applied Physics Letters **111**, 092601 (2017); 10.1063/1.4997097

[Broadband hot-carrier dynamics in three-dimensional Dirac semimetal \$\text{Cd}_3\text{As}_2\$](#)

Applied Physics Letters **111**, 091101 (2017); 10.1063/1.4985688

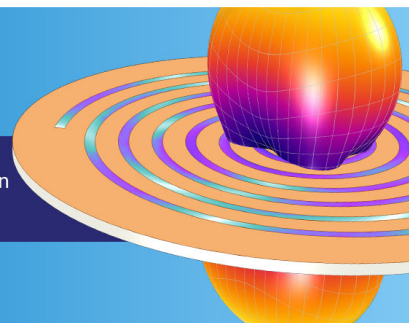
**COMSOL
CONFERENCE
2018 BOSTON**

Discover the power of multiphysics simulation.

COMSOL

OCTOBER 3-5
Boston Marriott Newton

Register Now ▶



Terahertz radiation enhanced emission of fluorescence from elongated plasmas and microplasmas in the counter-propagating geometry

Fabrizio Buccheri,¹ Kang Liu,¹ and Xi-Cheng Zhang^{1,2,a)}

¹The Institute of Optics, University of Rochester, Rochester, New York 14627, USA

²International Institute of Photonics and Optoinformatics, ITMO University, St. Petersburg 199034, Russia

(Received 14 June 2017; accepted 20 August 2017; published online 29 August 2017)

Remote sensing is one of the major challenges for Terahertz (THz) radiation applications, due to the THz wave attenuation by the atmosphere water vapor during its propagation. THz-Radiation-Enhanced-Emission-of-Fluorescence (REEF) is a THz air-photonics technique that has the potential to bypass this issue, by having the sought-after THz spectral fingerprints carried from the target to the operator by ultraviolet light, which experiences low absorption in the atmosphere. This technique has been previously demonstrated when the THz radiation and the laser excitation are focused collinearly, namely, the co-propagating geometry. However, the co-propagating geometry is not a favorable configuration for practical stand-off detection. Therefore, further exploration on alternative sensing geometries is still required. Herein, we report the interaction of broadband THz radiation with plasmas induced by a counter-propagating laser beam, which is a more desirable geometry for remote sensing. We have found that in the counter-propagating geometry, the maximum amplitude of the REEF signal is comparable to that in the co-propagating case, whereas the time resolved REEF trace significantly changes. By performing the study with different plasmas, we observed that in the counter-propagating geometry, the shape of the REEF trace depends strongly on the plasma length and electron density. A theoretical model suggesting that the densest volume of the plasma does not contribute to the fluorescence enhancement is proposed to reproduce the experimental measurements. Our results further the understanding of the THz-plasma interaction and highlight the potential of the THz-REEF technique in plasma diagnostic applications. Published by AIP Publishing. [<http://dx.doi.org/10.1063/1.4990143>]

Remote sensing is one of the most sought-after applications in terahertz (THz) sciences. The ability of THz radiation to identify chemical compounds through most dielectric packaging materials, hence differentiating the harmful from the harmless, is appealing to homeland security applications.^{1–3} Furthermore, the richness of information obtainable in this spectral region is welcomed in astronomy and environmental monitoring.^{4,5} However, the propagation of THz pulses through the atmosphere is severely affected by the absorption and dispersion, mostly caused by the presence of water vapor.⁶ In 2010, an “all optical” approach was demonstrated by Liu *et al.* allowing the coherent detection of THz pulses at a distance greater than 10 m.^{7,8} Their technique employs plasmas induced by ultrafast near infrared (NIR) laser pulses as the sensor for THz radiation. Specifically, the time evolution of the THz pulse is encoded in the fluorescence emission from the plasma through the process known as Terahertz Radiation Enhanced Emission of Fluorescence (THz-REEF).⁹ Due to the high atmospheric transparency for both the NIR laser pulses and the fluorescence radiation (ultraviolet), as well as the omnidirectional emission pattern of the fluorescence, the technique has been considered as a promising candidate for THz remote sensing.

The coherent detection of THz radiation facilitated by the REEF mechanism has been reported for the case of THz and NIR pulses propagating collinearly, i.e., co-propagating scheme.^{7,9} However, this interaction geometry is not applicable

in most stand-off THz sensing applications, where the THz wave is back-reflected from the target, illuminating the plasma sensor induced by a forward-propagating NIR laser pulse. Since in this case the THz pulse and the optical pulse are propagating in the opposite direction, this configuration is referred to as the counter-propagating scheme.

In this letter, we describe the interaction of coherent broadband THz radiation with plasma induced by a counter-propagating laser beam through the REEF mechanism. The fluorescence enhancement resulting from the THz radiation illumination was temporally resolved and measured for plasmas of different lengths, from $\sim 630 \mu\text{m}$ to $\sim 45 \mu\text{m}$.

Following a method similar to that employed by Liu *et al.* in Refs. 7 and 9, the setup implements the standard pump-probe THz time-domain spectroscopy technique¹⁰ with the relative time delay Δt between the pump and the probe pulses controllable through a motorized linear stage. The laser employed was Spectra Physics Hurricane (800 nm center wavelength, 100 fs pulse duration, 0.8 mJ pulse energy, and 1 kHz repetition rate). Intense single cycle THz pulses with a peak field of $\sim 90 \text{ kV/cm}$ were obtained via optical rectification in LiNbO₃ with tilted pulse front geometry.¹¹ The THz radiation was collected and refocused onto the plasma formed by focusing the optical beam. The plasma fluorescence is imaged into the input slit of a grating monochromator and measured with a photomultiplier tube (PMT) placed at its output slit or from the side into a gated intensified CCD (iCCD) camera (PIMAX3 Princeton Instruments). As a reference, the THz time-domain waveform was also

^{a)}xi-cheng.zhang@rochester.edu

measured by electro-optic (EO) sampling.¹² Through flip mirrors, the setup could be easily switched between the co-propagating and counter-propagating geometries, both of which are shown in Fig. 1(a).

First, the comparison between the REEF traces in both geometries for the case of elongated plasma is presented. More specifically, the plasma was generated by focusing 150 μJ laser pulses with a plano-convex (PC) lens with a 4 in. effective focal length (EFL). The resulting plasma had a length of $\sim 630 \mu\text{m}$. The plasma length is defined as the Full Width Half Max (FWHM) of the longitudinal cross-section of the plasma fluorescence image as measured with the iCCD camera. The REEF trace is obtained by measuring the intensity of the fluorescence emission line centered at 337 nm which belongs to the second positive band system of N_2 , as a function of the time delay, Δt , between the THz and the optical pulses. This particular emission line was chosen since it provides the REEF trace with the best signal-to-noise ratio in our experimental setup. The comparison between the REEF traces measured by the PMT in both configurations is shown in Fig. 1(b). Those plots depict the absolute fluorescence enhancement, ΔI_{FL} , obtained by subtracting the background fluorescence, i.e., the fluorescence intensity in the absence of THz radiation, from the signal measured with the THz radiation, as a function of Δt . In both cases, the fluorescence signal starts increasing when the THz pulse begins to overlap temporally with the optical pulse at the plasma location. In both configurations, the fluorescence enhancement magnitude, defined as the difference between the maximum value of the fluorescence intensity and the fluorescence background, is similar. However, the co-propagating trace (orange, dashed) shows a rapid increase of fluorescence with a timescale comparable to the THz pulse time duration, while the counter-propagating one exhibits a gentler slope with the rising time close to 10 ps. Notice that the interpretation of the time delay is different for the two schemes. In the co-propagating one, Δt is the time delay between the peaks of the two pulses as they travel in the same direction. Positive values are defined such that the THz pulse leads the optical pulse. Considering that the optical pulse is much

shorter than the THz pulse, in this geometry, the optical pulse is sensing the THz pulse. In the counter-propagating case, for different values of Δt , the THz pulse and the optical pulse meet at different locations of the plasma. Δt is arbitrarily defined equal to zero when the two pulses meet at the center of the plasma. In this geometry, the THz pulse is actually sensing the plasma at different times during its evolution. In the counter-propagating geometry, the rising time of the REEF trace depends on the length of the plasma, the longer the plasma the longer the rising time, resulting in a trace shape much different compared with the co-propagating one. Moreover, the slope of the co-propagating trace shows a distinctive feature, as shown in the inset of Fig. 1(b), which originates from the typical bipolar waveform of a single cycle THz pulse. The derivative of the curve yields the time-dependent THz pulse intensity as previously demonstrated by Liu and Zhang.⁹ However, for the case of elongated plasma generated by the 4 in. EFL lens, the counter-propagating trace is smooth and featureless.

As seen in Fig. 1(b), the rising time of the fluorescence enhancement ΔI_{FL} is faster in the co-propagation geometry and much slower in the counter-propagating one. In the latter case, the rising time depends on the longitudinal extension of the plasma. Longer plasmas result in a longer interaction time of the THz pulse with the ionized medium, therefore resulting in a slower rising time for ΔI_{FL} . To explore this phenomenon in more detail, we shortened the dimension of the plasma by changing the focal length of the focusing optics to the point of creating microplasmas. With 2 in. EFL and 1 in. EFL plano-convex lenses, we obtained microplasmas of lengths 100 μm and 45 μm , respectively. It is important to notice that the fluorescence spectra depend strongly on the laser intensities used to create the plasmas. In particular, for sufficiently high laser intensities, the molecular lines employed to measure the REEF signal are submerged by a broad super-continuum emitted several ns after the onset of ionization,¹³ with the result of rendering the measurement of the REEF signal significantly noisier.

The time-resolved REEF traces measured by PMT of the plasmas obtained with three different focusing elements, 4 in., 2 in. and 1 in. EFL, are plotted in Fig. 2. A co-propagating REEF curve with 4 in. EFL lens induced plasma (orange, dashed) is plotted together with each counter-propagating curve as a reference. As expected, when the plasma length decreases, the rising time of the fluorescence enhancement curve gets shorter. However, different from the case of elongated plasmas created by the 4 in. EFL lens, the curves obtained with the microplasmas display a distinctive undulation on the slope. While it is tempting to attribute this feature to the time-evolution of THz waveform, this conclusion is not supported by the much slower time scale at which this undulation evolves.

In order to interpret the origin of the shape of the REEF traces obtained in counter-propagating geometry with the microplasmas, we modified the mathematical expression describing the REEF traces in co-propagating geometry in the limit of high pressure gas⁹ to include also the space dependencies. The resulting expression for the plasma fluorescence enhancement ΔI_{FL} is

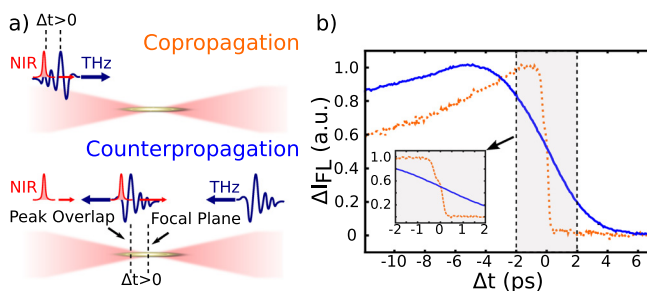


FIG. 1. (a) Depiction of the two interaction geometries. Top: in co-propagating geometry, the THz (blue) and the NIR (red) pulses travel in the same direction. Δt is the time delay between the two. Bottom: in counter-propagating geometry, the THz and NIR pulses travel in opposite directions. In this case, Δt corresponds to the THz pulse and NIR pulse meeting at different locations. (b) Plasma fluorescence intensity enhancement as a function of Δt in co-propagating (orange, dashed) and counter-propagating (blue, solid) geometries measured by PMT. Both curves are normalized to one. The absolute ratio between the maxima of the counter-propagating and co-propagating trace is 0.8. The onset shows a zoom of the curves for Δt between -2 and 2 ps.

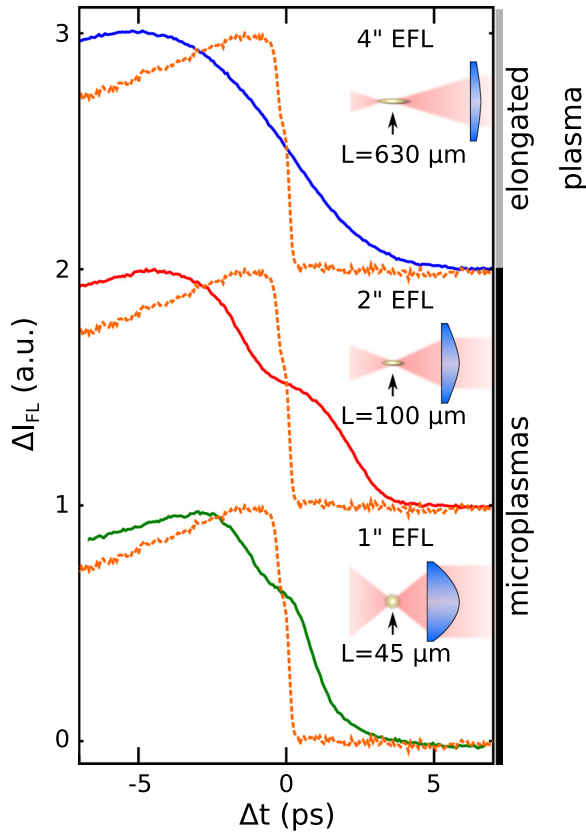


FIG. 2. Plasma fluorescence intensity enhancement as a function of Δt from plasmas obtained with the following optic components: 4 in. EFL plano-convex lens (blue, solid); 2 in. EFL plano-convex lens (red, solid); 1 in. EFL plano-convex lens (green, solid). The plots are offset for clarity. Each trace in counter-propagating geometry is plotted together with the one in co-propagating geometry obtained with the 4 in. EFL plano-convex lens (orange, dashed). Each curve is normalized to one.

$$\Delta I_{FL}(\Delta t) \propto \int \int_{-\infty}^{+\infty} dt dz n_{e,eff} \left(z, t - \Delta t \mp \frac{z}{c} \right) E_{THz}^2 \left(z, t - \frac{z}{c} \right), \quad (1)$$

where $n_{e,eff}$ is the effective electron density contributing to the fluorescence intensity change through THz-REEF and E_{THz} is the THz pulse electric field. By changing the sign in front of the propagation term $\frac{z}{c}$ inside of $n_{e,eff}(z, t - \Delta t \mp \frac{z}{c})$, the equation describes the cases of co-propagating (minus sign) and counter-propagating (plus sign) geometries. Through a least squares fitting algorithm, Eq. (1) was employed to retrieve hypothetical electron density spatial profiles $n_{e,eff}(z)$ that would result in the measured REEF traces in the cases of elongated plasma and the two microplasmas. For this purpose, we used the time dependence for n_e discussed in Ref. 9 and the THz electric field measured with EO sampling. The fitted curves and the respective computed plasma profiles are shown in Fig. 3. In the same figure, the computed plasma profiles are compared with the plasma fluorescence profile imaged from the side with the iCCD camera (Pimax 3, Princeton Instruments) using a gate time of 3 ns.

Instead of representing the actual electron density spatial distribution, the point-and-dash curves, Figs. 3(b), 3(d), and 3(f), are to be interpreted as the effective electron densities contributing to the REEF signals. In the case of elongated

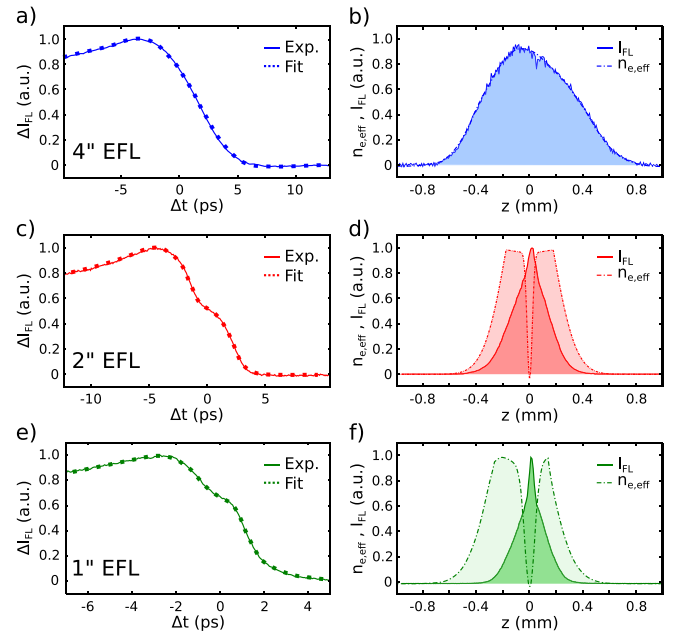


FIG. 3. Experimental (solid line) and numerical fitted (dashed line) plasma fluorescence intensity enhancement as a function of Δt in counter-propagating geometry for the following focusing conditions (a) 4 in. EFL PC lens; (c) 2 in. EFL PC lens; (e) 1 in. EFL PC lens; in figures (b), (d), and (f), the solid lines represent the integration of the plasma fluorescence intensity along the radial dimension as measured with the iCCD camera, whereas the point-and-dash lines are the numerically evaluated plasma effective electron densities producing the dashed curves plotted in (a), (c), and (e).

plasma, the effective electron density well matches with the fluorescence profile measured with the iCCD camera, therefore indicating that all the plasma volume contributes to the REEF interaction. However, the computed $n_{e,eff}$ and the measured fluorescence profiles differ dramatically in the cases of the smaller plasmas. In particular, those curves suggest that the denser part of the plasma has very little contribution to the fluorescence enhancement, whereas the biggest contribution is due to the interaction of the THz wave with the outer region of the plasma, where the electron density is lower. This could be qualitatively explained by two physics phenomena: (i) the volumes with the highest electron densities are the ones presenting the highest degree of ionization of the air molecules. It is therefore plausible that the contribution of those volumes to the THz-REEF signal is very small, as the density of electronic states right below the continuum (~ 100 meV), which are the ones contributing to the THz induced fluorescence enhancement,⁹ is greatly reduced for highly ionized molecules. (ii) As the fluorescence intensity enhancement peculiar to the REEF detection mechanism is the result of the interaction of the THz radiation with a formed plasma⁹ and the estimated characteristic ionization times in our experiment are less than 200 fs,¹⁴ one should also consider the skin effect. For values of electron densities higher than 10^{16} cm⁻³, which are achieved in the microplasmas generated in our experiments, the plasma frequency becomes greater than 1 THz. Frequencies below that value are not allowed to propagate through the plasma, but they decay exponentially within a length defined by the skin depth of the plasma at the specified frequency. The skin depth gets smaller as the electron density increases. For the estimated electron densities of the experiment and the peak frequency

of the input THz pulse (0.7 THz), the skin depth in the densest volume is as low as $5 \mu\text{m}$. Therefore, the densest part of the plasma is screened from the incoming THz pulse and does not contribute to the THz-REEF signal.

The possibility of resolving the THz intensity evolution in the counter-propagating geometry is however allowed by the theory for plasmas short enough to time-resolve field changes in the order of typical THz field oscillation times. A microplasma with a length of $15 \mu\text{m}$ would result in a time resolution of 50 fs, therefore allowing to accomplish this goal. As the THz-REEF process appears to require lower electron densities, the practical difficulty is that the fluorescence signal from such a short and low density plasma would be very small and close to the noise level of many optical detectors.

Another option could be to use a counter-propagating scheme with a long plasma and, instead of measuring the fluorescence with a “bucket detector,” which integrates the fluorescence intensity over the plasma volume, one could spatially resolve the fluorescence with a camera from the side. Figure 4 shows this arrangement in which the plasma fluorescence spatial distribution is obtained with a gated iCCD camera synchronized with the laser. The plasma is imaged from the side through a narrowband filter centered at 337 nm, in order to reject scattered light from the laser [Fig. 4(a)]. The gate time of the iCCD was chosen to be 3 ns, the shortest possible available with our instrument. The mapping of the pixel size into real space dimensions is obtained through the calibration of the images using a $100 \mu\text{m}$ pinhole as the target.

For a fixed value of Δt such that there is interaction between the THz pulse and the plasma, the spatially resolved fluorescence enhancement distribution can be obtained by subtracting the image taken when the THz pulse is illuminating the plasma from one when it is not. The plasma profiles with and without THz illumination and the retrieved fluorescence enhancement distribution corresponding to the peak of the PMT measured counter-propagating REEF trace ($\Delta t = -7.3 \text{ ps}$) are plotted in Fig. 4(b) as solid black, dashed black, and red lines, respectively.

The fluorescence enhancement curve [red dashed plot in Fig. 4(b)] obtained with this procedure is analogous to the temporally resolved REEF trace measured with the PMT in the co-propagating geometry [orange dashed trace

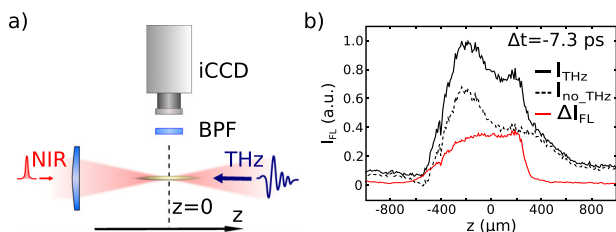


FIG. 4. (a) Experimental setup for taking the fluorescence images. The NIR (red) and THz (blue) pulses travel in opposite directions. The plasma is imaged from the side with an iCCD camera through a narrowband filter (BPF) centered at 337 nm. (b) Plasma fluorescence cross-sections with (black) and without (dashed, black) THz illumination. The red curve is the spatially resolved fluorescence enhancement calculated by subtracting the fluorescence profile with and without THz illumination.

in Fig. 1(b)]. In principle, the temporal resolution of this arrangement is limited by the spatial resolution of the imaging system, which can certainly allow us to resolve time-scales less than 50 fs. However, with our instrument we were not able to observe any feature in the slope of the fluorescence enhancement curve [like the one shown in Fig. 1(b) inset], and therefore, we did not prove that the technique could indeed resolve the THz field oscillation. A possible explanation is that during the exposure time of the camera of 3 ns, the plasma rearranges spatially smearing out the finest spatial features encoding the evolution of the THz pulse. Further investigation with cameras allowing shorter exposure time is needed.

In conclusion, in this letter, the interaction of THz pulses in counter-propagating geometry was demonstrated with both elongated plasmas and microplasmas through the REEF mechanism.

The REEF traces in counter-propagating geometry for elongated plasma do not visibly contain any feature related to the time evolution of the measured THz pulse. In the case of microplasmas, however, the REEF trace shows distinctive features in the slope. Those features, together with the rising time of the fluorescence enhancement, can be reproduced with the computation of hypothetical effective electron density distributions, suggesting that the densest volumes of the plasma do not contribute to the THz-REEF signal. Further experiments are necessary to confirm this hypothesis with the help of fast and high resolution CCD cameras and further manipulation of the plasma. The results presented herein suggest that the counter-propagating REEF is a good candidate as a tool for plasma diagnostics, for it essentially allows the THz radiation as a probe to sense the electron density and dimension of the plasma in question. Finally, two suggestions to improve the temporal resolution of the REEF technique in the counter-propagating geometry are given, which might allow through future investigation to enable the resolution of the THz field oscillation and advance the techniques for THz remote sensing.

Our research was sponsored by the Army Research Office and was accomplished under Grant No. W911NF-16-1-0436. The views and conclusions contained in this document are those of the authors and should not be interpreted as representing the official policies, either expressed or implied, of the Army Research Office or the U.S. Government. The U.S. Government is authorized to reproduce and distribute reprints for Government purposes notwithstanding any copyright notation herein.

¹H.-B. Liu, Y. Chen, G. J. Bastiaans, and X.-C. Zhang, *Opt. Express* **14**, 415 (2006).

²M. R. Leahy-Hoppa, M. J. Fitch, X. Zheng, L. M. Hayden, and R. Osiander, *Chem. Phys. Lett.* **434**, 227 (2007).

³A. G. Davies, A. D. Burnett, W. Fan, E. H. Linfield, and J. E. Cunningham, *Mater. Today* **11**, 18 (2008).

⁴J. F. Federici, B. Schulkin, F. Huang, D. Gary, R. Barat, F. Oliveira, and D. Zimdars, *Semicond. Sci. Technol.* **20**, S266 (2005).

⁵M. Tonouchi, *Nat. Photonics* **1**, 97 (2007).

⁶Y. Yang, M. Mandehgar, and D. R. Grischkowsky, *IEEE Trans. Terahertz Sci. Technol.* **1**, 264 (2011).

⁷J. Liu, J. Dai, S. L. Chin, and X.-C. Zhang, *Nat. Photonics* **4**, 627 (2010).

- ⁸K. Liu, F. Buccheri, and X.-C. Zhang, *Phys. Chin. Wuli* **44**, 492 (2015).
- ⁹J. Liu and X.-C. Zhang, *Phys. Rev. Lett.* **103**, 235002 (2009).
- ¹⁰M. Van Exter, C. Fattinger, and D. R. Grischkowsky, *Opt. Lett.* **14**, 1128 (1989).
- ¹¹K.-L. Yeh, M. C. Hoffmann, J. Hebling, and K. A. Nelson, *Appl. Phys. Lett.* **90**, 171121 (2007).
- ¹²Q. Wu and X.-C. Zhang, *Appl. Phys. Lett.* **67**, 3523 (1995).
- ¹³F. Martin, R. Mawassi, F. Vidal, I. Gallimberti, D. Comtois, H. Pépin, J. C. Kiefer, and H. P. Mercure, *Appl. Spectrosc.* **56**, 1444 (2002).
- ¹⁴V. A. Kostin, I. D. Laryushin, A. A. Silaev, and N. V. Vvedenskii, *Phys. Rev. Lett.* **117**, 035003 (2016).